Extreme waves analysis based on atmospheric patterns classification: an application along the Italian coast

Francesco De Leo[1], Sebastián Solari[2], and Giovanni Besio[1]

[1]Dept. of Civil, Chemical and Environmental Engineering - University of Genoa, Genoa, 16145, Italy
[2]Instituto de Mecánica de los Fluidos e Ingenieria Ambiental - Universidad de la República, Montevideo, 11300, Uruguay

Correspondence: Francesco De Leo (francesco.deleo@edu.unige.it)

Abstract.

The identification of homogeneous populations of data prior to perform Extreme Value Analysis (EVA) is advisable in all fields of sciences. When performing EVA on sea storms, it is also recommended to have an insight on the atmospheric processes behind the occurrence of the extremes, as this might facilitate the interpretation and ultimately use of the results.

5   In this work, a "bottom-up" approach for the identification and classification of the atmospheric processes producing extreme wave conditions is revisited, and applied to several locations among the Italian buoy network. A methodology is given for classifying samples of significant wave height peaks in homogeneous subsets, and for the computation of the overall extreme values distribution starting from the distributions fitted to each single subset. From the obtained results, it is concluded that the proposed methodology is capable of identifying clearly differentiated subsets driven by homogeneous atmospheric processes,

10 and it allows to estimate high return-period quantiles consistent with those resulting from the usual EVA. Two well-known cyclonic systems are identified as most likely responsible of the extreme conditions detected in the investigated locations. These systems are analysed in the context of the Mediterranean sea atmospheric climatology, and compared with those figured out by previous researches developed in similar frameworks.

1   Introduction

15 The extreme value theory is widely used for the analysis of extreme data in most of the geophysical applications. It allows to estimate extreme (un-observed) values, starting from available records or modelled data which are assumed to be independent and identically distributed (Coles, 2001). It is therefore crucial to identify homogeneous datasets complying with the above mentioned requirement before performing the EVA of a given physical quantity.

When dealing with directional variables, it is common to group the data according to different directional sectors (Cook

20 and Miller, 1999; Forristall, 2004), being such approach recommended as well in many regulations (API, 2002; ISO, 2005; DNV, 2010, among others). However, the use of directional sectors involves certain drawbacks. First, it cannot be employed for variables being not characterized by incoming directions (such as storm surge or rainfall). Second, data showing the same direction may be due to different forcing; in the frame of wave climate, an example is that of waves propagating in shallow waters, affected by refraction and/or diffraction. Finally, the borders of the directional sectors are often subjectively defined,

25 without verifying if the data belonging to each subset are homogeneous and independent with respect to those of the other
sectors (see Folgueras et al., 2019, where they tackled this issue and proposed a methodology to overcome it).

An alternative approach to classify the extremes implies resorting to the atmospheric circulation conditions they are driven
by, associating each extreme event to a particular weather pattern (referred to as WP). Such approach has been already deep-
seated in atmospheric sciences for the analysis of precipitations, snowfalls, temperature, air quality and winds (Yarnal et al.,
30 2001; Huth et al., 2008, among others). Nevertheless, there are few studies linking weather circulation patterns with the most
likely induced sea states (e.g., wave climate and storm surge). Holt (1999) classified WPs leading to extreme storm surges
in the Irish Sea and the North Sea. Guanche et al. (2013) simulated multivariate hourly sea state time series in a location in
the northwester Spanish coast, starting from the simulation of weather pattern time series. Dangendorf et al. (2013) linked
the atmospheric pressure fields with the sea level in the German Bight (southeastern North Sea). Pringle et al. (2014, 2015)
35 investigated how extreme wave events may be tied to synoptic-scale circulation patterns in the east coast of South Africa.
Camus et al. (2014) proposed a statistical downscaling of sea states based on weather types, then applied to a couple of
locations in the Atlantic coast of Europe to hindcast the wave climate during the twentieth century plus modelling it under
different climate change scenarios. The latter methodology was improved by Camus et al. (2016), and further used by Rueda
et al. (2016) for analysing significant wave height maxima. Solari and Alonso (2017) used WP classification to perform EVA
40 of significant wave heights in the south-east coast of South America.

Except for Rueda et al. (2016) and Solari and Alonso (2017), none of the previous works focused on exploiting WP classi-
fication methodologies for defining homogeneous datasets to be further employed for EVA. However, the two methodologies
differ in several aspects. Rueda et al. (2016) dealt with daily maxima significant wave heights along with surface pressure
fields and pressure gradients, averaging over different time periods and applying a regression-guided classification to define
45 100 WPs. They subsequently fit a Generalized Extreme Value distribution, estimating an Extremal Index from the daily max-
ima significant wave height of each WP, from which they rebuilt the overall distribution of annual maxima (referred to as AM
H_s). Despite the proposed methodology is able to reproduce the AM H_s distribution, with such a large number of WPs it may
be difficult to detect the most relevant physical processes behind the occurrence of extreme wave conditions. Furthermore, as
shown in Rueda et al. (2016), even though a large number of WPs was considered, only a few happened to significantly affect
50 the EVA, as most of the WPs resulted to be associated to mild wave conditions. Finally, to retain daily maxima does not ensure
the data to be independent, thus implying the need to use the Extremal Index. Solari and Alonso (2017) introduced instead a
"bottom-up" scheme: they first selected a series of independent extreme sea states; then, they identified a reduced number of
WPs that allows to group the selected data into homogeneous populations. A small number of WPs makes it easier to link the
different subsets of extremes with known climate forcing. Above all, to work with independent peaks allows to rely on the
55 classic and well known extreme value theory, with no need to refer to additional indexes and/or more complex models that may
be unfamiliar for many analysts.

In this paper, the methodology of Solari and Alonso (2017) is revisited and applied to several wave datasets along the Italian
coastline. The objective of this research is twofold: (i) to explore how the definition of homogeneous subsets, based on WP,

affects the estimation of H_s extreme values; (ii) to characterize the identified WPs in the framework of the Mediterranean

60 Region (MR) cyclones climatology.

The paper is structured as follows: in Sect. 2 we introduce the data and describe the methodology developed; results are presented and discussed in Sect. 3; finally, in Sect. 4 conclusions are summarized and further developments are introduced.

2 Data & Methods

2.1 Wave and atmospheric data

65 This work takes advantage of eight hindcast points located in the Italian seas, as shown in Fig.1. This choice allowed to test the reliability of the proposed methodology under different local wave climates. In fact, the selected points are differently located along the Italian coastline, and, being exposed to different fetches, they are characterized by peculiar wave conditions. The same locations were taken into account by Sartini et al. (2015), where they performed an overall assessment of the different frequency of occurrence of the extreme waves affecting the Italian coasts. Table 1 reports the names, depths, and coordinates

70 of the selected locations.

The points correspond to as many buoys belonging to the Italian Data Buoy Network (Rete Ondametrica Nazionale or "RON", Bencivenga et al., 2012), which collected directional wave parameters over different periods between 1989 and 2012. Unfortunately, most of the buoys are characterized by significant lacks of data due to malfunctions and maintenances of the devices. We therefore referred to hindcast data, since such a widespread lack of data would imply a loss of reliability for

75 the following analysis. We relied to the hindcast of the Department of Civil, Chemical and Environmental Engineering of the University of Genoa (http://www3.dicca.unige.it/meteocean/hindcast.html; Mentaschi et al., 2013, 2015), providing wave parameters on a hourly base from 1979 to 2018 over the whole Mediterranean sea. Data were validated against the records of the buoys (when available); more details can be found in Mentaschi et al. (2013, 2015). The wind data used to drive the wave generation model were derived from the NCEP Climate Forecast System Reanalysis for the period from January 1979

80 to December 2010 and CFSv2 for the period from January 2011 to December 2018, downscaled over the MR along with the pressure fields through the model Weather Research and Forecast (WRF-ARW version 3.3.1, see Skamarock, 2009; Cassola et al., 2015, 2016). These wind velocities data were used here to feed the cluster analysis of the wave peaks, while the pressure data were used for the analysis of the climatology related to the identified WPs (as explained in Sect. 2.3 and Sect. 2.4, respectively).
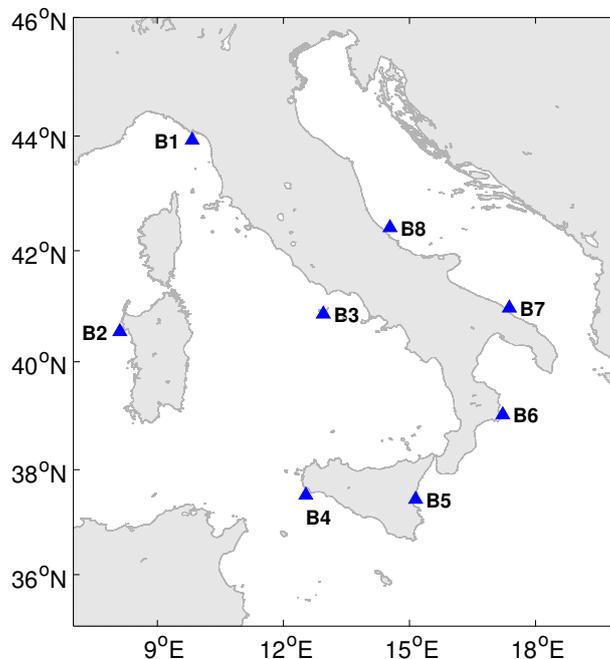
Figure 1. Study area and investigated locations with their respective codes

CODE	LON	LAT	DEPTH [m]	NAME
B1	9.8278	43.9292	83.8	La Spezia
B2	8.1069	40.5486	99.7	Alghero
B3	12.9500	40.8667	242.0	Ponza
B4	12.5333	37.5181	90.8	Mazara del Vallo
B5	15.1467	37.4400	65.4	Catania
B6	17.2200	39.0236	611.7	Crotone
B7	17.3778	40.9750	80.0	Monopoli
B8	14.5367	42.4067	55.8	Ortona

Table 1. Lon/lat coordinates and depths of the hindcast locations employed in the study (reference system: WGS84)

2.2 Extreme events selection

For each location, wave height peaks were selected through a Peak Over Threshold (POT) approach, and in particular by using a time moving window. This approach works as follows. First, the whole series of H_s is spanned through a time moving window of given width; second, when the maximum of the data within the window happens to fall in the middle of the window itself,

it is retained as a peak; finally, in order to get rid of the peaks which are not related to severe sea states, a first H_s threshold is
90 chosen and only peaks exceeding this threshold are retained for further analysis.

In this study, for each location the width of the moving window was set equal to one day, meaning that the inter-arrival time
between two successive storms is at least equal to one day. The threshold was fixed as the 95th percentile of the resultants
peaks. This ensured to maintain a uniform approach for all the locations, efficiently capturing the different features of the local
wave climates. Beside the significant wave heights, we retained as well the waves mean incoming directions corresponding to
95 the peaks (θ_m), which were used for analysing the outcomes of the clustering algorithm. Finally, for each peak we extracted
the mean sea level pressure field (MSLP) and surface wind fields for several time lags (0, 6, 12 24, 36, and 48 hours earlier
with respect to the peak's date), over the whole MR. Wind fields were used to classify the selected peaks due to their parent
WP, as described in the following section; MSLP fields were used instead for the post-processing and climatological analysis
of the results.

2.3 Extreme events classification: definition of weather patterns

The classification of extreme events is based on surface wind fields ($\bar{u}_w$) observed in the whole MR during the hours before and
concomitant to the time of the peaks. In order to define the spatial and temporal domains to be taken into account, we looked
at the correlation maps between the wind velocities and the H_s peaks for different time lags. Correlations were evaluated over
a sub-grid of the atmospheric hindcast, with nodes spaced of $0.5°$ both in longitude and latitude. To compute the correlation
105 between H_s and $\bar{u}_w$ series is not straightforward, as the former variable is scalar and the latter is directional. To tackle this
issue, we followed the procedure suggested by Solari and Alonso (2017). Given a time lag Δt, the wind at every node (i,j) is
defined by its zonal and meridional components $(u_x, u_y)_{(i,j,\Delta t)}$; the correlation between H_s peak series and the time lagged
surface wind speed at any given node is then estimated as the maximum of the linear correlations obtained by projecting the
wind speed series in all the possible directions:

$$110 \quad \rho_{(i,j,\Delta t)} = \max_{0 \le \theta < 2\pi} \left\{ \rho \left(H_s; \bar{u}_{(i,j,\Delta t,\theta)} \right) \right\} \tag{1}$$

where $\rho_{i,j,\Delta t}$ is the resulting correlation for node (i,j) at time lag Δt, ρ refers to linear correlation function, $u_{(i,j,\Delta t,\theta)}$ is
the surface wind speed projected along direction θ according to Eq (2):

$$\bar{u}_{(i,j,\Delta t,\theta)} = u_{x(i,j,\Delta t)} cos(\theta) + u_{y(i,j,\Delta t)} sin(\theta) \tag{2}$$

in this way not only a maximal correlation is obtained for every node, but also the direction corresponding to the maximal
115 correlation, estimated as:

$$\hat{\theta}_{\rho(i,j,\Delta t)} = \underset{0 \le \theta < 2\pi}{\mathrm{argmax}} \left\{ \rho \left(H_s; \bar{u}_{(i,j,\Delta t,\theta)} \right) \right\} \tag{3}$$

The correlation maps computed with Eq. (1), allowed to evaluate the spatial domain and the time lags for which $\bar{u}_w$ is
significantly correlated to (i.e., directly affecting) the resulting wave peaks at a given location.

Once the spatial and time domain of the wind fields producing the peak wave conditions were defined, the wind fields were

120 used for clustering and classifying the extreme events. To this end, the *k-means* algorithm was used, fed with the normalized wind fields. *k-means* is aimed at partitioning a N-dimensional population into k sets (clusters) on the basis of a sample, in order to minimize the intra-cluster variance (MacQueen et al., 1967). The normalization of the wind fields sought to reduce the influence of the intensity of the wind speed on the classification, so that only the spatial form of the field and its time evolution were taken into account. Note that the values of H_s did not play any role in the classification of the peaks but the identification

125 of the point in time of the wind fields.

2.4 Analysis of the WPs climatology

Once the wind fields, and therefore peak H_s series, were grouped into k clusters, the MSLP corresponding to the events within each cluster were averaged and the position of the lowest pressure was recorded, for all the Δt taken into account. This allowed us to track the paths of the averaged low pressure systems corresponding to each cluster, defining in turn the respective WP.

130 At a second time, the dynamics of the systems were compared with those of the cyclones typically detected in the Mediterranean sea (Trigo et al., 1999; Lionello et al., 2016), while the frequency of occurrence of the events of different clusters were compared with the outcomes of Sartini et al. (2015). The number of clusters needed to group the series into was defined for every location by looking at the outcome of the cluster analysis: when an increase from k to $k+1$ clusters did not further lead to a new clearly differentiated WP, the research was stopped and k was used for the cluster analysis of that particular location.

135 ### 2.5 Extreme value analysis

The EVA were performed independently over the subsets of H_s peaks resulting from the cluster classification. We followed the methodology proposed by Solari et al. (2017), where the threshold for the POT analysis was estimated as the one maximizing the p_{value} of the upper tail Anderson-Darling test. Then, once the threshold is estimated (i.e. a subset of the peaks within a given WP is defined), the three parameters of the GPD are estimated through the L-moments method, and the return-period

140 (T_r) quantiles of the variable under investigation are computed. In this work, in order to estimate the overall T_r-H_s curve and its confidence intervals from the GPDs fitted to each WP, a bootstrapping approach was implemented (see Algorithm 1). Algorithm 1 shows a pseudocode summarizing the bootstrapping procedure. First, N_{boot} series of H_s, each N_{years} long, are generated for every WP. Second, the series generated for the different WPs (N_{WP} per location) are combined in order to obtain one single N_{years} long series for each of the N_{boot} simulations. Third, an empirical relation between T_r and H_s (i.e. an

145 empirical cumulative distribution function or ECDF) is estimated from each one of the N_{boot} series. Lastly, expected value and confidence intervals of H_s are estimated from the N_{boot} ECDFs for several return periods.

The method assumes a Poisson-GPD model for each WP and that the realizations of different WP are independent from each other. This independence hypothesis was evaluated by estimating the correlation between the annual number of peaks associated to each WP.

Algorithm 1 Computational scheme of empirical extreme values curves and its confidence intervals

---

for $j \leftarrow 1, N_{boot}$ **do**

    for $i \leftarrow 1, N_{WP}$ **do**

        $\{H_s\}_{i,0} \leftarrow random(GPD, \hat{\theta}_{(i,0)}, N_i)$

        $\hat{\theta}_i \leftarrow fit(GPD, \{H_s\}_{i,0})$

        $\{N_{simu}\}_i \leftarrow f_i(\hat{\lambda}_i, N_{years})$

        $\{H_s\}_i \leftarrow random(GPD, \hat{\theta}_i, \{N_{simu}\}_i)$

    end for

    $\{H_s\}_j \leftarrow [\{H_s\}_i, i = 1 \dots N_{WP}]$

    $H_s \leftarrow sort(\{H_s\}_j)$

end for

$H_s = \hat{f}(T_r) \leftarrow \{f_i\}$

$C.I. \leftarrow \{f_i\}$

Comments:

N_{boot} is the number of bootstrapping repetitions

N_{WP} is the number of WP

$\hat{\theta}_{(i,0)}$ are the parameters of the GPD estimated from the original sample

N_i is the length of the original sample of H_s peaks within the WP

$\hat{\lambda}_i$ is the yearly number of events of the ith WP

N_{years} is the number of years simulated; it must be larger that the maximum return period to be analized

N_{simu} is the numer of events in N_{years} obtained for the ith WP

$H_s = f(T_r)$ is the empirical Hs-Tr curve

---

150   For a given location, the overall work-flow can be summarized as follows:

    – selection of a series of H_s peaks through a POT approach

    – selection of the wind field data to be employed in the clustering algorithm (i.e. Δt and spatial domain)

    – classification of the H_s peaks due to the $k - means$ algorithm

    – definition of a suitable number (k) of WPs

155   – averaging of the MSLP corresponding to the peaks of each WP, for each Δt taken into account

    – performing EVA over the single subsets

    – computation of the overall long term distribution through a bootstrapping technique

This methodology was applied to all the hindcast locations shown in Fig. 1. In this paper, for the sake of clarity, just the results of the locations B4 (Mazara del Vallo) and B7 (Monopoli) are shown and discussed. Indeed, just one WP was necessary

160 for classifying the peaks in La Spezia and Alghero (B1 and B2), thus no further analysis were performed. Among the locations left, we simply selected the locations furthest from each other in the East-West direction. All the results related to the other locations can be found in the supplementary material.

3   Results and discussions

Once the series of H_s peaks is selected, the first step of the proposed methodology requires to define the domains of $\bar{u}_w$ in

165 time and space due to the outcomes of the correlation analysis between the two parameters. Figure 2 shows the correlation maps for B7 for different time lags, along with the directions leading to the maximum values of correlation in each node. It is interesting to see how $\hat{\theta}$ for Δt=0 hours are distributed along the nodes characterized by similar values of ρ. Actually, even though the values of $\hat{\theta}$ come from a purely statistical analysis (i.e., they were computed with Eq. (3)), their spatial distribution follow that of a typical cyclone. Velocities happen to be uniformly oriented along the nodes characterized by the higher values

170 of ρ, close-to-tangential to a circle centred on the nodes showing instead lower values of ρ. This allows to get a first insight on the predominant process most likely affecting the wave climates of the investigated locations, as it will be discussed further on this paper. On the contrary, the analysis of the correlations between H_s and $\bar{u}_w$ reveals that the areas characterized by similar values of ρ are not uniformly distributed in the neighbourhood of the points considered. It is therefore difficult to uniquely contour the nodes to be taken into account for the successive analysis. As regards the time step, correlations rapidly decrease

175 for Δt longer than 12 hours, after which no evidence of significant ρ can be observed. The same outcomes apply for all the other locations taken into account.

Results suggest that the events shall be linked with broader circulation patterns. In view of the above, it was decided to refer to the whole MR and time lags of 0 and 12 hours for the purposes of peaks classification.
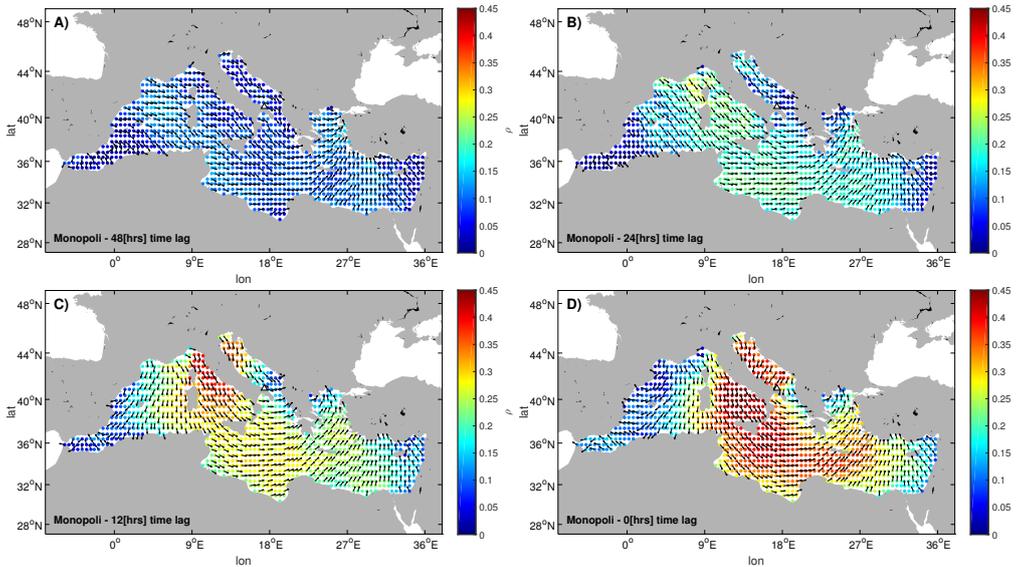
Figure 2. Correlations between H_s and $\bar{u}_w$ in location B4 for different time lags. Panel A): Δt equals 48 hours; panel B): Δt equals 24 hours; panel C): Δt equals 12 hours; panel D): Δt equals 0 hours

Once the spatial and temporal limits of the wind fields to be used in the $k-means$ were defined, we performed a sensitivity
180 analysis over the resultant average MSLP belonging to each cluster, among the total amount of tested clusters (k). Two clusters
were needed to detect different systems at all the sites but Alghero and La Spezia, where a single pattern was enough to describe
the local extreme waves. For the other locations, to increase k did not lead to systems significantly diverging from those already
defined. The reason for such a small number of resulting WPs has to be found in the nature of the H_s employed in the analysis.
Indeed, these are associated to extreme sea states, which are most likely driven by atmospheric phenomena developing along
185 well-defined and fixed tracks.

Figures 3 and 4 show the averaged pressure fields corresponding to both the clusters and Δt in B4 and B7 hindcast points.
Here, two main systems can be clearly distinguished: i) a low moving SW-NE towards the Balkan area (say WP#1) and ii) a
low moving NW-SE (henceforth referred to as WP#2).
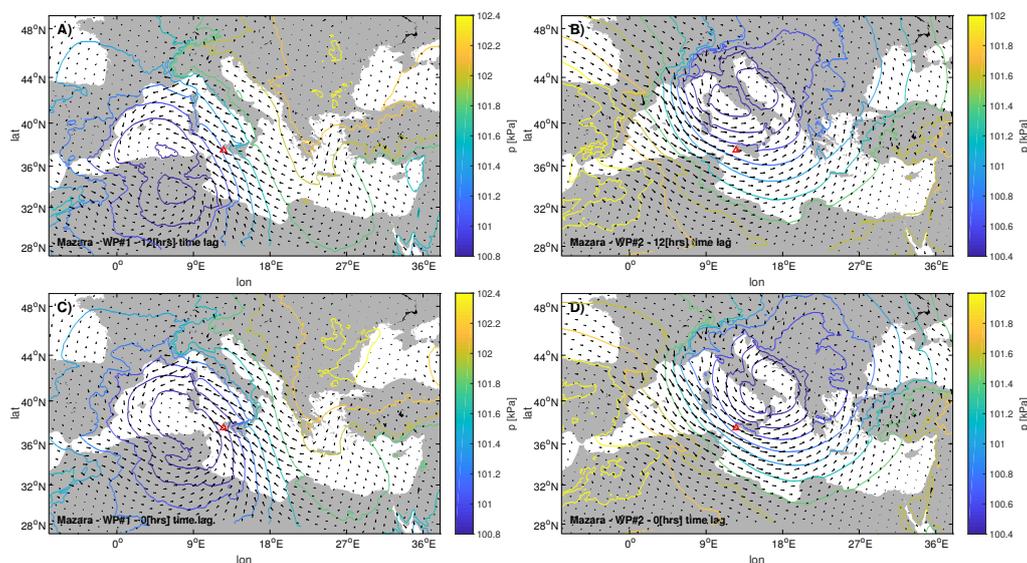
Figure 3. Average MSLP for the H_s peaks in Mazara del Vallo (B4). Panel A): WP#1, Δt equals 12 hours; panel B) WP#2, Δt equals 12 hours; panel C): WP#1, Δt equals 0 hours; panel D): WP#2, Δt equals 0 hours

Let us first focus on WP#2. Low pressure moves SE from the central Europe, crossing the Adriatic sea and decreasing its
190 intensity once it gets to the south Balkan area, where it stops until it finally dissolves. As regards WP#1, the cyclogenesis most
likely takes place in the east area of north Africa, with cyclones first approaching the west coastline of Italy while moving NE.
The paths of WP#1 and WP#2 show evident similarities with well known cyclones typically forming and departing from two
of the most active cyclogenetic regions in the MR, respectively the lee of the Atlas mountains and the lee of the Alps (Trigo
et al., 1999). Actually, WP#2 seems to follow the Genoa system path that usually moves down to the Albanian and Greek
195 coasts, while that of WP#1 is characteristic of the Sharav depression, moving north-eastward toward the Greek region (Flocas
and Giles, 1991; Trigo et al., 1999, 2002). The same paths characterize the lows of the WPs detected in all the investigated sites
(see the supplementary material). A summary of the lows position at the two different Δt can be appreciated in Fig 5, reporting
the tracks of both the WP#2 and WP#1 systems in all the sites; in the latter case, no results for B1 and B2 are available, since
all the peaks happened to belong to a single WP.
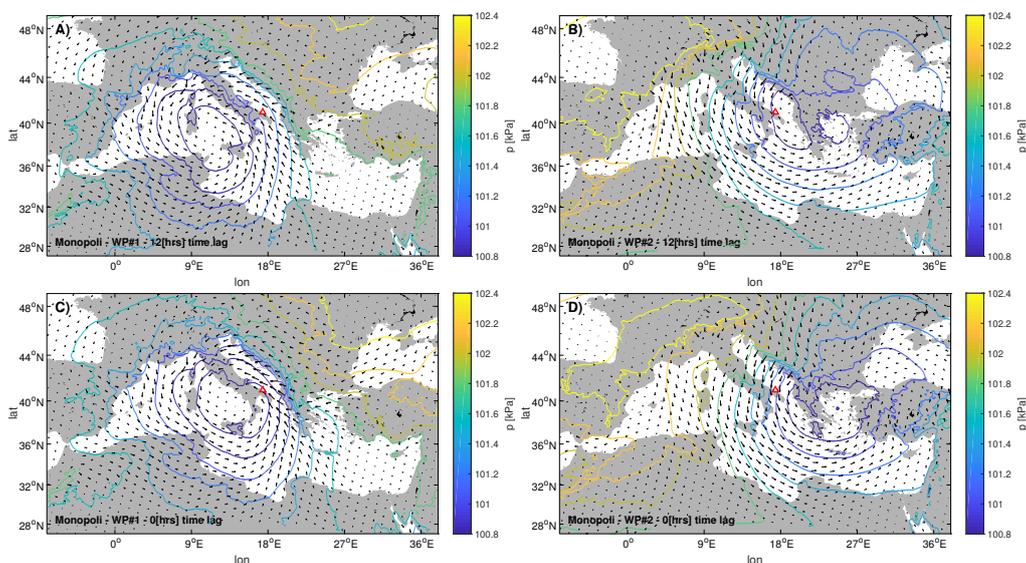
Figure 4. Average MSLP for the H_s peaks in Monopoli (B7). Panel A): WP#1, Δt equals 12 hours; panel B) WP#2, Δt equals 12 hours; panel C): WP#1, Δt equals 0 hours; panel D): WP#2, Δt equals 0 hours
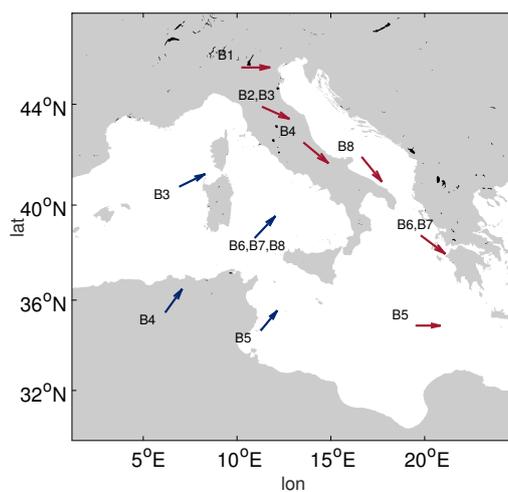
Figure 5. Time evolution of the center of the low pressure for the different WP identified for each buoy. In blue WPs with lows traveling northeastward (WP#1); in red WPs with lows traveling east-or southeastward (WP#2)

200   It is interesting to see how the WP#2 low get across the investigated sites in a precise chronological order, crossing first the northernmost locations and then those next to the south Balkan area where the cyclone actually ends its run. As such, we took as a reference four buoys affected by WP#2 at different times, evaluating the time lag between their respective peaks generated by such system. We considered the extreme series of B4, computing for each storm the time lag between peak at the buoy and peaks occurring in B2 and B1 (occurring earlier) and B6 (occurring later); distributions of the time lags are shown in Fig. 6.
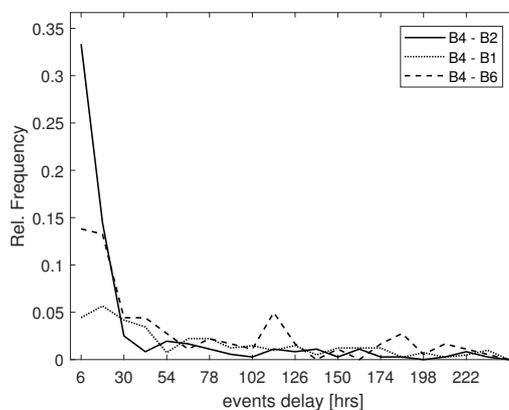
Figure 6. Relative frequency of the events' delay for B2, B1 and B6. Referring series is that of B4

205   Looking at Fig. 6, it is evident how the majority of the events' delays between B4 and the other investigated points fall within about forty hours. We therefore evaluated the average MSLP fields for time lags up to 48 hours before and after the storms occurring at the reference location, tracking the low pressure centre evolution. Results show how the cyclone runs out in a couple of days, the center of the low travelling for approximately 1600 kilometres, with a resulting speed of $\sim$33 km h^{-1} (see Fig. 7). Both the lifetime of the identified cyclone and the speed it moves at are compatible with the features of the cyclones

210   most frequently encountered in the MR (Lionello et al., 2016). Unfortunately, as regards WP#1, an equally clear path cannot be detected, as the average lows apparently arise simultaneously in most of the points taken into account. We therefore not further characterize the mean evolution of the MSLP fields characterizing the events of WP#1.
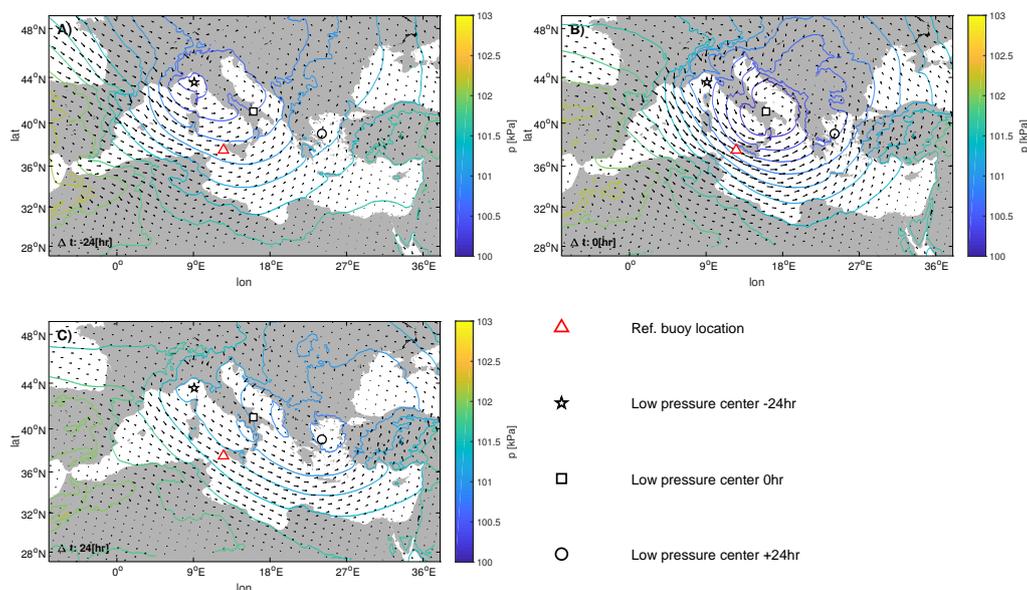
Figure 7. WP#2: average MSLP evolution with respect to the reference dates of the events in B4 (underlined with the red triangle)

The characterization of the two systems is reflected in the frequency of occurrence of the storms, with peaks belonging to different subsets showing as well distinctive seasonality. From the results shown in Fig. 8, it can be noticed how WP#2 peaks mainly occur in winter, whereas the events of WP#1 are characterized by two milder intra-annual peaks of occurrence, spread among the spring and autumn months. The intra-annual cycle of the WP#1 events further suggest a direct link with the Sharav cyclones, which show similar seasonal fluctuations; as regards the WP#2 peaks, even though the storms of the Genoa low are more uniformly distributed along the year, the most intense events precisely occur during winter, as it happens in the above mentioned locations (details can be found in Lionello et al., 2016).

Figure 9 summarizes the results of the monthly frequency of occurrence of the extremes in all the investigated locations, grouped according the WP. For each location, frequencies were normalized in the 0-1 space with respect to the total amount of peaks, in order to be able to compare outcomes defined over different ranges.
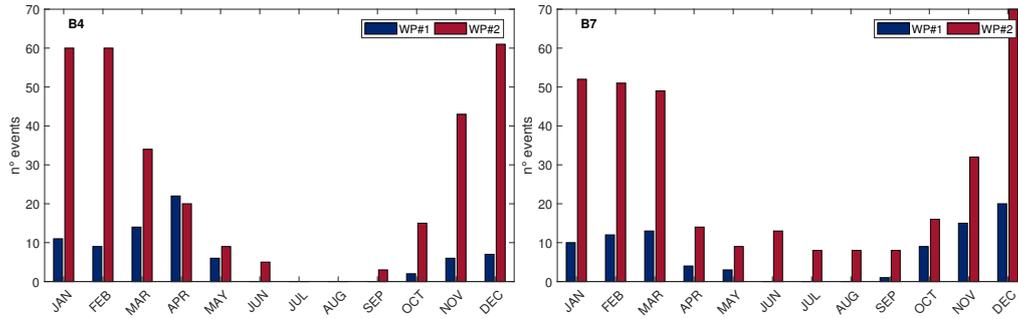
Figure 8. Monthly number of events for different WP. Left panel: B4; right panel: B7
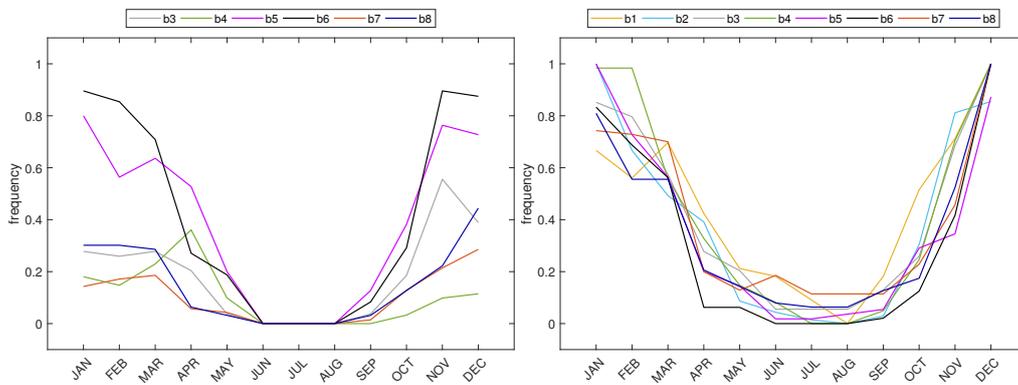
Figure 9. Normalized monthly frequency of occurrence of the extremes. Left panel: events belonging to WP#1; right panel: events belonging to WP#2.

It can be noticed how the relative weight of WP#1 events on the overall peaks distributions increases moving south. Points in the northernmost locations (B1 and B2) apparently are not influenced by the WP#1 system, and their extreme waves are

225 actually linkable just to WP#2. Moving to the southernmost locations (B5 and B6), no significant differences in the seasonality of the two patterns' events can be appreciated; in these two buoys none of the two systems shows a prevailing frequency of occurrence for the induced storms.

The aforementioned behavior may be justified by looking at the location of the investigated points (see Fig. 1): lows moving north-eastward directly run over B5 and B6, marginally affect B7, B8, B4 and B3, whereas they do not interest at all B1 and

230 B2. However, position of the buoys with respect to the cyclones' paths is not the only relevant variable. Indeed, it may happen that peaks related to the same WP show distinct frequencies of occurrence, for instance the events related to WP#1 in B6 and

B7; in this case, the predominant parameter seems to be the fetch length, which for B7 is very limited with regards to the NE incoming waves (precisely related to the first weather circulation pattern).

The WPs that are defined in the present study show common characteristics with those qualitatively identified by Sartini
235 et al. (2015) in a seasonal variability analysis of extreme sea waves. In particular, the same WP was identified in B1 and B2, linking the extremes with the Gulf of Genoa cyclogenesis WP type. As Sartini et al. (2015) noted, even if cyclones in the Genoa Gulf are a constant feature over the whole year, those connected at the extreme events are the ones characterized by the lowest value in MSLP. These findings (i.e., higher values during the winter rather than in spring and summer time) were observed in the southern Thyrrenian Sea as well (for instance in B4) and in the Central Thyrrenian Sea (B3). In the latter case, we found
240 a more marked seasonal variation of the extremes, as the two resultant WPs are well separated between winter and autumn. Intra-annual variability was observed also for B7, while the analysis carried out by Sartini et al. (2015) did not reveal this kind of behaviour; analogously, B5 and B8 buoy revealed the presence of two distinct WPs, while the previous analysis identified just one cyclogenesis system. These differences may be justified in the first place by the different peaks selection (a moving window for this study, while Sartini et al., 2015, use a partial duration series approach). Moreover, evaluation of the seasonality
245 follows completely different algorithms: the present study directly applies a clustering technique over the selected peaks, while the former analysis used the peaks to model a time dependent distribution, further characterizing their seasonality on the basis of the values of the distribution coefficient aroused from the fitting procedure.

Another interesting outcome regards the characteristics of the extremes differentiated due to the parent clusters following the $k-means$ algorithm. Fig. 10 shows the covariates H_s and θ_m of the selected peaks belonging to each WP.
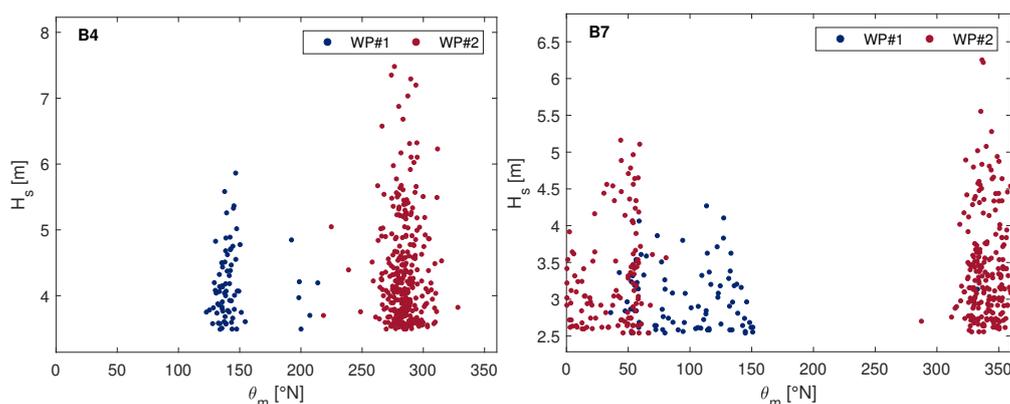
Figure 10. Scatter plot of H_s and θ_m due to different WP. Left panel: B4; right panel: B7

250 Looking at the scatter plots, it is evident how the proposed methodology allows to differentiate the sea storms according to the directional frames of the local wave climate. This particularly applies for locations characterized by a bimodal distribution with respect to the waves' incident direction (like B4, where is clear the presence of two peaks corresponding to SE and NW). On the other hand, when the waves' direction is more uniformly scattered over a given sector, it is not unusual that different

climate forcing result in the same wave direction; this can be noticed in B7, where θ_m-H_s scatters belonging to different
255   patterns are partially overlapped, thus a directional classification is not straightforward and most probable would not be able to
differentiate the storms due the cyclones generating them.

Finally, Fig. 11 shows the T_r-H_s curves, comparing the results obtained directly from the whole set of peaks with those
obtained from the single-WP distributions, combined by means of Algorithm 1 (i.e., omni-WP curves).

The omni-WP curves show a striking agreement with those carried out through the analysis of the whole dataset without
260   WP classification; in both the locations B4 and B7 it can be even appreciated a narrowing of the confidence intervals, meaning
a reduction in the total variance for the long-term estimates. Actually, the curve related to B4 show a slight deviation between
the two approaches ($\simeq$ 30 cm over the 200 year wave); however, such small magnitudes imply relative errors of $\simeq$ 4% with
respect to the omni-WP curves, and can be therefore considered as an uncertainty inherent in this kind of computations (see
e.g., Borgman and Resio, 1977, 1982, stating that reliable long term estimates can be carried out just up to three times the
265   years the length of the original dataset).
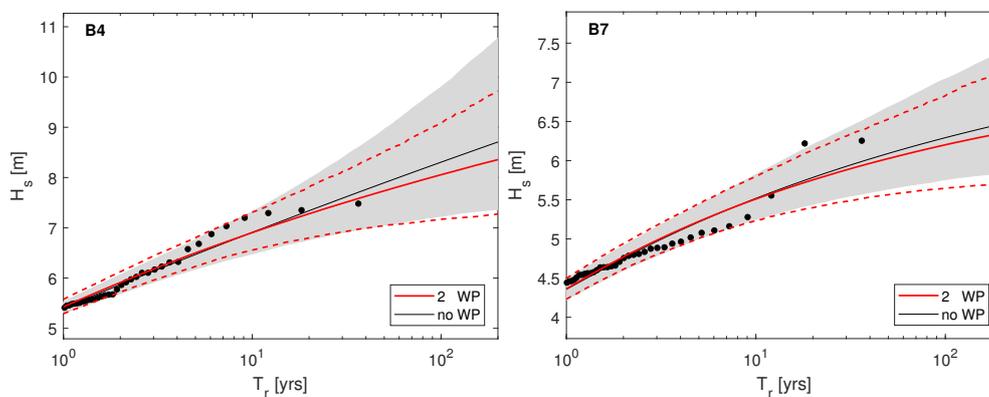
Figure 11. Omni-WP extreme value distributions of H_s obtained from the whole set of peaks (black) and from combining single-WP
distributions (red), along with 90% confidence intervals (grey shadow and red dashed lines, respectively). Left panel: B4; right panel: B7

These results seem to reinforce the validity of developing the omni-WP curve under the hypothesis of independence between
the events of different WPs. In this case, the independence hypothesis was to some extent corroborated by the low correlations
values attained by the intra-clusters annual frequency of occurrence for all the locations: -0.17, 0.23, -0.13, -0.11, -0.34, 0.13
for B5, B6, B4, B7, B8 and B3 respectively).

270   **4   Conclusions**

Results on the analysis of the extremes reveal how different weather circulation patterns may lead to sea storms having, on
average, unique characteristics. Such homogeneous features (both in terms of frequency of occurrence and significant wave

heights) suggest that the extreme distributions of H_s shall be singularly evaluated for each WP, the starting datasets being homogeneous and independent with respect to each other.

275   The methodology here introduced allows the classification of extreme wave events (or other oceanic variables) into homogeneous subgroups according to the atmospheric processes generating them. By focusing solely on extreme events, the proposed classification method results in a reduced number of circulation or weather patterns, which facilitates their physical interpretation as well as their linkage with the climatology of the area.

The method, as presented here, does not contemplate the inclusion of trends and inter- or intra-annual cycles. However,
280   the extension of the methodology in this direction is straightforward, as the methods previously developed for non-stationary analysis (see e.g., Sartini et al., 2015) could be applied without major complexities to each of the subsets that are obtained from the classification. On the contrary, it is not obvious how to proceed in the selection of the number of patterns to be considered. Here this number was chosen following a qualitative analysis of the results, which was viable for the case study analysed. However, this approach is not always feasible, and sometimes it might be necessary to (at least) resort to a sensitivity analysis
285   of the results, as long as a quantitative methodology is not available for the definition of the number of clusters.

For the analysed locations, the proposed methodology led to the identification of two well known cyclonic systems, characteristic of the atmospheric circulation on the Mediterranean Sea, as the origin of the extreme wave events affecting the Italian shores. When extreme events are classified according to their meteorological origin, there is a great confidence of working with homogeneous samples, thus being in compliance with the main hypothesis underlying the EVA. Nevertheless, the prac-
290   tical consequences of the classification in terms of the omni-WP extreme distribution are relatively limited: although in some cases a narrowing in the confidence intervals was achieved, in general the distribution obtained by following the two different approaches was very similar. However, it must be kept in mind that the classification could facilitate other aspects of the analysis not included in this work, such as the multivariate analysis of extreme events.

Code and data availability. The algorithms used in this work were developed in Matlab®. The codes and the hindcast data employed are
295   available upon request. Please contact FDL at: francesco.deleo@edu.unige.it.

Author contributions. FDL developed the algorithms and wrote the paper. SS coordinated the work and contributed to developing the codes and writing the paper. GB provided the data, analysed the results in the frame of the MR climatology, and revised the writing of the paper.

Competing interests. The authors declare that they have no conflict of interest.

Acknowledgements. Mobility of Francesco De Leo has been financed by the University of Genoa through the program "Fondo Giovani

300   17/18".

Authors deeply acknowledge Francesco Ferrari of the University of Genoa for the help in processing the meteorological hindcast.

References

API: API RP 2A-WSD: Recommended Practice for Planning, Designing and Constructing Fixed Offshore Platforms-Working Stress Design, American Petroleum Institute, 2002.

305 Bencivenga, M., Nardone, G., Ruggiero, F., and Calore, D.: The Italian data buoy network (RON), Advances in Fluid Mechanics IX, 74, 321, 2012.

Borgman, L. and Resio, D.: Extremal prediction in wave climatology, in: Proceedings of Ports, ASCE, New York, vol. I, pp. 394–412, 1977.

Borgman, L. E. and Resio, D.: Extremal statistics in wave climatology, Topics in ocean physics, 80, 439–471, 1982.

Camus, P., Menéndez, M., Méndez, F. J., Izaguirre, C., Espejo, A., Cánovas, V., Pérez, J., Rueda, A., Losada, I. J., and Medina, R.:
310 A weather-type statistical downscaling framework for ocean wave climate, Journal of Geophysical Research: Oceans, 119, 1–17, https://doi.org/10.1002/2014JC010141, 2014.

Camus, P., Rueda, A., Méndez, F. J., and Losada, I. J.: An atmospheric-to-marine synoptic classification for statistical downscaling marine climate, Ocean Dynamics, 66, 1589–1601, https://doi.org/10.1007/s10236-016-1004-5, http://dx.doi.org/10.1007/s10236-016-1004-5, 2016.

Cassola, F., Ferrari, F., and Mazzino, A.: Numerical simulations of Mediterranean heavy precipitation events with the WRF model: analysis
315 of the sensitivity to resolution and microphysics parameterization schemes, Atmospheric Research, 164-165, 210–225, 2015.

Cassola, F., Ferrari, F., Mazzino, A., and Miglietta, M.: The role of the sea on the flash floods events over Liguria (northwestern Italy), Geophysical Research Letters, 43, 3534–3542, 2016.

Coles, S.: An Introduction to Statistical Modeling of Extreme Values (Springer series in statistics), Springer-Verlang, 2001.

Cook, N. J. and Miller, C. A.: Further note on directional assessment of extreme winds for design, Journal of Wind Engineering and Indus-
320 trial Aerodynamics, 79, 201–208, https://doi.org/10.1016/S0167-6105(98)00109-3, https://www.nat-hazards-earth-syst-sci-discuss.net/nhess-2018-198/, 1999.

Dangendorf, S., Wahl, T., Nilson, E., Klein, B., and Jensen, J.: A new atmospheric proxy for sea level variability in the southeastern North Sea: observations and future ensemble projections, Climate Dynamics, https://doi.org/10.1007/s00382-013-1932-4, http://link.springer.com/10.1007/s00382-013-1932-4, 2013.

325 DNV: DNV-RP-C205: Environmental Conditions and Environmental Loads, Det Norske Veritas, 2010.

Flocas, A. and Giles, B.: Distribution and intensity of frontal rainfall over Greece, International journal of climatology, 11, 429–442, 1991.

Folgueras, P., Solari, S., and Losada, M. Á.: The selection of directional sectors for the analysis of extreme wind speed, Natural Hazards and Earth System Sciences, 19, 221–236, 2019.

Forristall, G. Z.: On the use of directional wave criteria, Journal of waterway, port, coastal, and ocean engineering, 130, 272–275, 2004.

330 Guanche, Y., Mínguez, R., and Méndez, F. J.: Climate-based Monte Carlo simulation of trivariate sea states, Coastal Engineering, 80, 107–121, http://www.sciencedirect.com/science/article/pii/S0378383913000963, 2013.

Holt, T.: A classification of ambient climatic conditions during extreme surge events off Western Europe, International Journal of Climatology, 19, 725–744, https://doi.org/10.1002/(SICI)1097-0088(19990615)19:7<725::AID-JOC391>3.0.CO;2-G, 1999.

Huth, R., Beck, C., Philipp, A., Demuzere, M., Ustrnul, Z., Cahynová, M., Kyselý, J., and Tveito, O. E.: Classifications of at-
335 mospheric circulation patterns: recent advances and applications., Annals of the New York Academy of Sciences, 1146, 105–52, https://doi.org/10.1196/annals.1446.019, http://www.ncbi.nlm.nih.gov/pubmed/19076414, 2008.

ISO: ISO 19901-1:2005: Petroleum and natural gas industries - Specific requirements for offshore structures - Part 1: Metocean design and operating considerations, International Organization for Standards, 2005.

Lionello, P., Trigo, I., Gil, V., Liberato, M., Nissen, K., Pinto, J., Raible, C., Reale, M., Tanzarella, A., Trigo, R., Ulbrich, S., and Ulbrich,
340   U.: Objective climatology of cyclones in the Mediterranean region: a consensus view among methods with different system identification
and tracking criteria, Tellus A, 68, 2016.

MacQueen, J. et al.: Some methods for classification and analysis of multivariate observations, in: Proceedings of the fifth Berkeley sympo-
sium on mathematical statistics and probability, vol. 1, pp. 281–297, Oakland, CA, USA, 1967.

Mentaschi, L., Besio, G., Cassola, F., and Mazzino, A.: Developing and validating a forecast/hindcast system for the Mediterranean Sea,
345   Journal of Coastal Research, SI 65, 1551–1556, 2013.

Mentaschi, L., Besio, G., Cassola, F., and Mazzino, A.: Performance evaluation of WavewatchIII in the Mediterranean Sea, Ocean Modelling,
90, 82–94, 2015.

Pringle, J., Stretch, D. D., and Bárdossy, A.: Automated classification of the atmospheric circulation patterns that drive regional
wave climates, Natural Hazards and Earth System Science, 14, 2145–2155, https://doi.org/10.5194/nhess-14-2145-2014, http://www.
350   nat-hazards-earth-syst-sci.net/14/2145/2014/, 2014.

Pringle, J., Stretch, D. D., and Bárdossy, A.: On linking atmospheric circulation patterns to extreme wave events for coastal vulnerability
assessments, Natural Hazards, 79, 45–59, https://doi.org/10.1007/s11069-015-1825-4, 2015.

Rueda, A., Camus, P., Méndez, F. J., Tomás, A., and Luceño, A.: An extreme value model for maximum wave heights based on weather
types, Journal of Geophysical Research, 121, 1–12, https://doi.org/10.1002/2015JC010952, 2016.

355   Sartini, L., Cassola, F., and Besio, G.: Extreme waves seasonality analysis: An application in the Mediterranean Sea, Journal of Geophysical
Research: Oceans, 120, 6266–6288, 2015.

Skamarock, W.: Coauthors, 2008: A description of the advanced research WRF version 3. NCAR Tech. Note, Tech. rep., NCAR/TN-475+
STR, 2009.

Solari, S. and Alonso, R.: A new methodology for extreme waves analysis based on weather-patterns classification methods, Coastal Engi-
360   neering Proceedings, 1, 23, 2017.

Solari, S., Egüen, M., Polo, M. J., and Losada, M. A.: Peaks Over Threshold (POT): A methodology for automatic threshold estimation using
goodness of fit p-value, Water Resources Research, 53, 2833–2849, 2017.

Trigo, I. F., Davies, T. D., and Bigg, G. R.: Objective climatology of cyclones in the Mediterranean region, Journal of Climate, 12, 1685–1696,
1999.

365   Trigo, I. F., Bigg, G. R., and Davies, T. D.: Climatology of cyclogenesis mechanisms in the Mediterranean, Monthly Weather Review, 130,
549–569, 2002.

Yarnal, B., Comrie, A. C., Frakes, B., and Brown, D. P.: Developments and prospects in synoptic climatology, International Journal of
Climatology, 21, 1923–1950, 2001.